Journal of Materials Chemistry A

Accepted Manuscript

This article can be cited before page numbers have been issued, to do this please use: L. K. Jagadamma, M. T. Sajjad, V. Savikhin, M. F. Toney and I. D. W. Samuel, *J. Mater. Chem. A*, 2017, DOI: 10.1039/C7TA03144K.

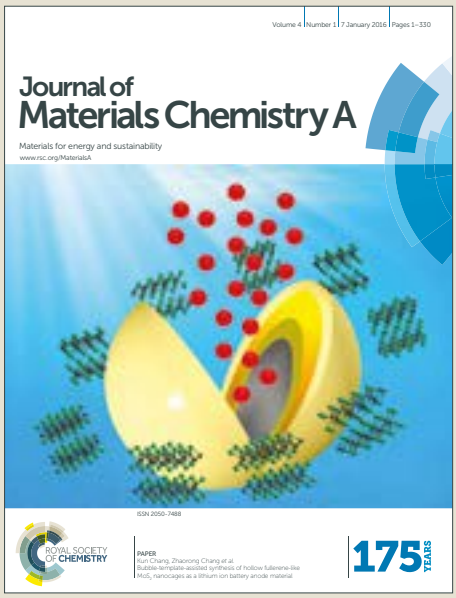

ROYAL SOCIETY OF CHEMISTRY

rsc.li/materials-a

DOI: 10.1039/C7TA03144K

Journal of Materials Chemistry A

ARTICLE

Correlating photovoltaic properties of PTB7-Th:$PC_{71}BM$ blend to photophysics and microstructure as a function of thermal annealing

Received 00th January 20xx,
Accepted 00th January 20xx

DOI: 10.1039/x0xx00000x

www.rsc.org/

Lethy Krishnan Jagadamma[1], *Muhammad T. Sajjad*[1], *Victoria Savikhin*[2, 3], *Michael F. Toney*[2], *Ifor D. W. Samuel*[1,*]

Selective optimisation of light harvesting materials and interface properties has brought breakthroughs in power conversion efficiency (11-12 %) of organic photovoltaics (OPVs). However to translate this promising efficiency to economically viable applications, long term stability is a fundamental requirement. A number of degradation pathways, both extrinsic and intrinsic, reduce the long term stability of OPVs. Here, the photovoltaic properties of a highly efficient bulk heterojunction PTB7-Th:$PC_{71}BM$ blend were investigated as a function of *ex-situ* thermal annealing. The changes in charge generation, separation, and transport due to thermal annealing were measured and related to changes in the microstructure and photovoltaic performance. A 30 % drop in power conversion efficiency of PTB7-Th:$PC_{71}BM$ blends upon thermal annealing at 150 °C was identified as mainly due to morphological instability induced by strong phase separation of donor and acceptor molecules of the blend films. Based on the insight gained from these investigations, enhanced thermal stability was demonstrated by replacing the $PC_{71}BM$ fullerene acceptor with the non-fullerene acceptor ITIC, for which power conversion efficiency dropped only by 9 % upon thermal annealing at 150 °C.

Introduction

Organic solar cells are a very promising and versatile photovoltaic technology because of their simple fabrication, flexible and thin form, tunablility of absorption properties and robust performance under a wide range of lighting conditions[1-4]. All these attributes make them suitable for a range of applications, such as being placed on irregularly shaped products; hence they are ideal energy sources for portable battery powered consumer electronics. Over a decade now, the focus of research for organic solar cells has been on increasing the power conversion efficiency (PCE). Single junction polymer solar cells with power conversion efficiencies of over 10 % have now consistently been achieved over the last two years - a longstanding target for commercialisation[5-12]. This has been made possible by directed development, research and systematic optimisation of low bandgap conjugated polymers, processing methods and interface engineering. The recently developed promising low bandgap conjugated polymers in this regard are PTB7-Th[8], PffBT4T-2OD[9], PBDB-T[10], blended with $PC_{71}BM$ to realise a near ideal nanoscale phase separation for efficient photovoltaic properties. OPV device architectures incorporating plasmonic nano-structures to maximise light absorption[13] and doping of the charge transporting layers[11] have further enhanced the power conversion efficiency of these blends. However, as discussed in the Unification Challenge[14] - which discusses realizing the objective of achieving stable, efficient, low cost polymer solar cells - the stability of organic solar cells should also be on par with power conversion efficiency and processability, otherwise the progress towards the application of the technology will remain slow. Though the simple solution processing and the possibility of roll to roll fabrication can ensure the cost effectiveness of this photovoltaic technology, stability is a great concern for organic solar cells. Accordingly, investigation of the stability of organic photovoltaic (OPV) blends is recently receiving more attention and standard stability testing protocols are now being implemented[15-19]. Among the highly efficient narrow bandgap donor polymers, the benzodithiophene (BDT) derivative based PTB7-Th mixed with fullerene $PC_{71}BM$ acceptor has reproducibly demonstrated power conversion efficiency greater than 10 % by different research groups[7, 10, 11, 20] and hence is an interesting candidate for further thermal processing and stability investigation.

The stability of organic solar cells is often studied by measuring the effect of chemical/photo/thermal processes on the power conversion efficiency. Chemical degradation of organic solar cells, due to water and/or oxygen from ambient air reacting with the active layer, is reported for systems like P3HT:PCBM[21, 22] and now needs to be understood and extended to OPV blends which have demonstrated lab scale PCE of 10 % and above. The inherent acidity of PEDOT:PSS, the most commonly used hole transport layer material in standard OPV architecture (causes it to react with ITO

[1]*Organic Semiconductor Centre, SUPA, School of Physics and Astronomy, University of St. Andrews, St. Andrews, Fife, KY16 9SS (UK)*
**Email - idws@st-and.ac.uk*
[2] *Stanford Synchrotron Radiation Lightsource (SSRL), SLAC National Accelerator Laboratory, Menlo Park, CA, USA*
[3] *Department of Electrical Engineering, Stanford University, Stanford, CA, USA*
Electronic Supplementary Information (ESI) available: [details of any supplementary information available should be included here]. See DOI: 10.1039/x0xx00000x

View Article Online
DOI: 10.1039/C7TA03144K

and the low work function of electrodes such as Al (making it react with ambient oxygen) are two important factors contributing towards the OPV performance degradation[14]. Inverted device architectures with thin oxide layers functioning as charge transport layers and high work function metal electrodes as anodes have been developed to improve stability and performance[14]. The photo-stability of PTB7-Th:$PC_{71}BM$ blends has been reported very recently and has shown that incomplete removal of DIO additive accelerates the photo-degradation of the OPV devices[23]. The structural ageing or degradation of nanoscale morphology of P3HT:$PC_{61}BM$ and PCDTBT:$PC_{71}BM$ organic solar cells was previously reported by Schaffer et al under *in-operando* conditions for a prolonged period of ~ 18 h. [24, 25]

To analyse the role of thermal effects on OPV blends, two aspects should be taken into consideration: the first is thermal annealing as a processing method for improving the photovoltaic performance, and, the second is the use of thermal annealing as a stressing method to probe the operational stability of an OPV blend. Considering the former aspect: thermal annealing can modify the nanoscale phase separation and crystallization of OPV blends, which impacts the efficiency of charge generation, extraction and operational stability. The optimised molecular packing and morphology of both the acceptor and donor is essential for efficient exciton transport (diffusion) and maximum charge carrier mobility to the electrodes. This has been demonstrated as an efficient method for systems such as P3HT:$PC_{61}BM$, where polymer P3HT is semi-crystalline.[26, 27] In the case of poorly ordered polymers such as PTB7-Th, characterised by weak intermolecular interaction, the suitability or applicability of such post processing techniques on the nano-scale morphology, phase behaviour, optical and electrical properties of PTB7-Th:$PC_{71}BM$ blend thin films has not been reported. In order to facilitate further increase in efficiency and applicability, it is vital that the factors governing the performance of these high efficiency OPV blends are identified and understood. A deeper understanding of thermal annealing effects on photovoltaic performance parameters of fill factor (FF), short-circuit current density (Jsc), open circuit voltage (Voc), and correlating these parameters with polymer orientation, packing structure, photophysics and phase separation of these blends, will help accelerate the understanding of how to manipulate the molecular arrangement of BHJ systems to achieve improved stability without compromising the power conversion efficiency. Though the focus of our work is thermal processing induced changes in the photovoltaic properties of PTB7-Th:$PC_{71}BM$ blends, the changes following the heating are also relevant to for long term thermal stability.

In this work, we have investigated the photovoltaic properties of PTB7-Th:$PC_{71}BM$ blend as a function of thermal annealing over a range of temperatures (from room temperature to 150 ^{o}C) and how the morphological, structural, charge transport and photophysical properties are contributing to the observed effect. An inverted device architecture was employed to avoid degradation of the ITO/PEDOT:PSS or Ca/Al contacts. *Ex-situ* thermal annealing process was applied only to the active layer of the PTB7-Th:$PC_{71}BM$ blend films, and not to the full organic solar cells. This was to exclude any influence of degradation of charge selective layers or metal contacts on the photovoltaic properties of PTB7-Th:$PC_{71}BM$ blends during the thermal annealing process. With increase in thermal annealing temperature from room temperature to 150 ^{o}C, the power conversion efficiency of the PTB7-Th: $PC_{71}BM$ blend based OPV devices decreases from 9.1 % to 6.85 %, mainly due to a drop in Jsc and FF. However, the open circuit voltage slightly improves from 0.77 V to 0.78 V. Since the active layer consists of a blend of a conjugated polymer and a small molecule, the phase separation and crystallization processes are complex and hence a range of characterisation methods has been employed to probe the possible reasons for the efficiency drop. The developed understanding will contribute towards enhancing the operational stability of OPVs based on this high efficiency blend system. Preliminary results on improved thermal stability of PTB7-Th:ITIC blend system, where ITIC is used as a non-fullerene acceptor, are also demonstrated.

Experimental section

Preparation of ZnO electron transporting layer

The electron transporting layer was an amorphous ZnO (a-ZnO) thin film of ~ 25 nm thickness[28]. The zinc oxide precursor solution (0.11 M) was prepared by dissolving equimolar ratios of zinc acetate dihydrate (ZAD) ($Zn(CH_3COO)_2.2H_2O$, Sigma Aldrich 99.9%) and monoethanolamine (MEA) ($NH_2CH_2CH_2OH$) in 2-methoxy ethanol ($CH_3OCH_2CH_2OH$, Sigma Aldrich 99.8%) at room temperature. The precursor solution was stirred continuously at room temperature for 24 hours to induce hydrolysis in air. After the hydrolysis in air, the precursor solution was spin coated on a cleaned ITO surface at 2000 rpm for 30 seconds. This was followed by annealing in air on a hotplate at 150 ^{o}C for 10 minutes.

Fabrication of PTB7-Th:$PC_{71}BM$ based inverted solar cells

Inverted solar cells were fabricated on pre-patterned ITO-coated glass. The ITO-coated glass substrates were cleaned in detergent (sodium dodecyl sulphate-SDS), ultra-sonicated in deionized water, acetone, isopropyl alcohol and exposed to Plasma Asher for 3 minutes. The PTB7-Th:$PC_{71}BM$ blend solution was prepared by dissolving in the ratio of 1:1.5 (by weight), with a total solid concentration of 25 mg/mL in chlorobenzene and 3vol% DIO. The solution was stirred at 60°C for ~8 h before deposition. The active layer was deposited by spin coating (1200 rpm, 45 s) on glass/ITO/a-ZnO substrates inside a nitrogen filled glove box. The resulting film thickness was approximately 150 nm as measured by profilometry. For investigating the *ex-situ* thermal annealing effects on PTB7-Th:$PC_{71}BM$ blend, the samples were left to dry for 20 minutes, then transferred to a hotplate set at different annealing temperatures of 70 ^{o}C, 100 ^{o}C, 120 ^{o}C and 150 ^{o}C, for 15 minutes. After 15 minutes, the samples were removed from the hotplate. All the processing related to the active layer was performed inside the glove box. The samples were loaded into a vacuum thermal evaporator (1 x10^{-6} mbar base pressure) in the glove box for thermally evaporating the hole transporting layer of MoO_x (7 nm) and anode Ag (100 nm) using a shadow mask. The active area of the devices was 0.08 cm^2 (4 mm × 2 mm).

Characterisation of solar cells

After the electrode deposition, the devices were encapsulated with a UV optical adhesive and a glass coverslip. The current–voltage characteristics were determined under an illumination intensity of 100 mW/cm^2 in air using an air mass 1.5 global (AM 1.5G) Sciencetech solar simulator and a Keithley 2400 source-measure unit. The illumination intensity was verified with a calibrated monosilicon detector and a KG-5 filter. The external quantum efficiency (EQE) measurements were performed at zero bias by illuminating the device with monochromatic light supplied from a Xenon arc lamp in combination with a dual-grating monochromator. The number of photons incident on the sample was calculated for each wavelength by using a silicon photodiode calibrated by national physical laboratory (NPL).

View Article Online
DOI: 10.1039/C7TA03144K

Characterisation of PTB7-Th:$PC_{71}BM$ active layer blend

The surface morphology of the of PTB7-Th:$PC_{71}BM$ films was characterised using atomic force microscopy (AFM). AFM images were obtained with a Bruker MultiMode 8 instrument in the tapping mode. NANOSENSORS™ PPP-NCSTR Si cantilever tips with force constant of 6–7 Nm^{-1} were used as AFM probes. Steady state absorption spectra of the blend films were recorded using a Varian Cary 300 spectrophotometer for the wavelength range of 300-800 nm. For this the active layer blend was deposited under identical conditions to those used for OPV devices, but on a fused silica disc. Time resolved photoluminescence (TRPL) spectra in the pico-nano seconds regimes were acquired with a synchroscan streak camera (C6860 from Hamamatsu). The excitation wavelength was from the frequency-doubled output of a Ti:sapphire laser, giving 400 nm, 100 fs full-width half-maximum pulses at 80 MHz. Samples for streak camera measurements were held under an active vacuum of ~10^{-5} mbar. The excitation wavelength used for the time - resolved PL measurements was 515 nm.

Grazing incidence wide angle X-ray scattering measurements were performed at Stanford Synchrotron Radiation Lightsource beamline 11-3. 12.735 keV photons were used with 2D scattering patterns recorded on a MARCCD detector. The beam center and sample-to-detector distance was calibrated using a Lanthanum Hexaboride standard. Scattering patterns were recorded as a function of the X-ray angle of incidence, with an angle of incidence of 0.14° or 0.2°. The former angle was chosen close to the critical angle to maximise intensity, whereas the latter angle was chosen well above the critical angle to minimise the effect of alignment error. Data acquisition times of 60 s were used, and 3 to 10 exposures were averaged to improve SNR. X-ray diffraction data were expressed as a function of the scattering vector, q, which is defined as $(4\pi/\lambda) \sin\theta$, where 2θ is the scattering angle and λ is the wavelength of the incident radiation. From Bragg's Law, $q=2\pi/d$, where d is a crystal repeat length (or in this case, intermolecular spacing).

Hole-only or electron-only diodes were fabricated using the architectures ITO/PEDOT:PSS/PTB7-Th: $PC_{71}BM/MoO_3$/Ag for holes and Al/ PTB7-Th: $PC_{71}BM$/LiF/ Al for electrons. The mobility was extracted by fitting the current density–voltage curves using the space charge limited current method (SCLC).

Results and discussion

Photovoltaic properties of the blend films

The photovoltaic properties of the PTB7-Th:$PC_{71}BM$ solar cells annealed at different temperatures are shown in Figure 1. The illuminated J-V curve (dark J-V curves in inset) in Figure 1a shows a clear trend of decreasing short circuit current density (Jsc) and fill factor (FF) resulting in an overall drop in power conversion efficiency from 9.1 to 6.85 % with increase in thermal annealing temperature from room temperature to 150 °C. In contrast, the open circuit voltage (Voc) shows a small increase. The FF drops from 71 to 62% with a corresponding decrease in Jsc from 16 to 13 mA/cm^2. Previous reports on thermal annealing of other efficient OPV blend systems of PCDTBT:$PC_{71}BM$, and PBDTTPD:$PC_{71}BM$, also displayed a decreasing PCE with thermal annealing[29, 30]. However, for the same temperature range, the drop in photovoltaic parameters (FF, J_{sc} and V_{oc}) was different from that observed for PTB7-Th:$PC_{71}BM$. This indicates the need to study the thermal processing effects and hence thermal stability of each efficient OPV blend separately. The shunt resistance decreases monotonically with increase in thermal annealing of PTB7-Th:$PC_{71}BM$ blend, and can account for the increased leakage current seen in dark J-V characteristics of high temperature thermally annealed blends [Table 1 and inset of Figure 1a]. Possible reasons for the reduction in photocurrent density and FF can be reduced exciton dissociation, poor charge separation efficiency, or decreased charge extraction efficiency and the increased recombination losses of the photo-generated charge carriers. In order to investigate the cause of the reduction in these photovoltaic properties, detailed microstructural and photophysical characterisation was performed as detailed below.

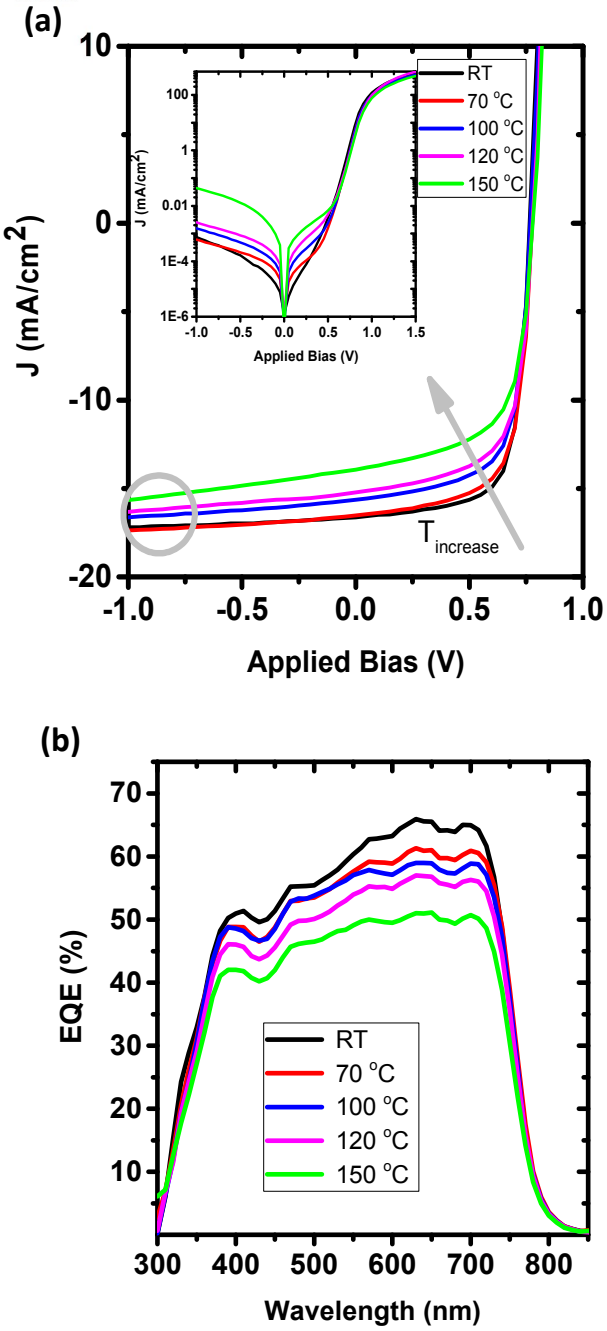

View Article Online
DOI: 10.1039/C7TA03144K

Figure 1. (a) J-V characteristics of the PTB7-Th:$PC_{71}BM$ blends as a function of thermal annealing. Inset shows the dark J-V characteristics (b) EQE spectra of the blend films as a function of thermal annealing.

Table 1: Photovoltaic performance parameters of the PTB7-Th:$PC_{71}BM$ blend as a function of thermal annealing temperatures. For each annealing temperature, the first row shows average photovoltaic parameters of 18 devices (and the standard deviation) and the second row shows the best device.

Annealing Temp. (°C)	J_{sc} (mA/cm²)	V_{oc} (V)	FF (%)	R_{sh} (Ωcm⁻²)	Rs (Ωcm⁻²)	PCE avg. (%)	PCE best (%)
RT	16.1(0.7)	0.77(0.01)	71.3(1.4)	1160(55)	3.14(0.54)	8.8(0.3)	
	16.6	0.77	71.5	1210	3.03		9.1
70	15.8(0.6)	0.77(0.01)	67.9(1.5)	688(99.8)	3.84(0.19)	8.3(0.4)	
	16.5	0.78	68.7	747	3.83		8.8
100	15.1±0.6	0.77(0.01)	67.8(1.7)	780(121)	3.78(0.45)	7.9(0.2)	
	15.6	0.77	68.2	620	3.45		8.2
120	14.3±0.7	0.78(0.01)	65.6(0.7)	561(74)	4.86(0.69)	7.3(0.4)	
	15.2	0.78	66.2	529	4.18		7.8
150	13.5±0.5	0.77(0.01)	62.2(2.4)	472(63)	5.37(0.53)	6.7(0.3)	
	13.9	0.78	63.1	464	5.20		6.9

To identify the potential loss mechanisms that limit the overall PCE of OPV devices as a function of thermal annealing, light intensity (**I**) dependent J-V curves were measured and analysed. The relation between short circuit current and light intensity follows a power law relation

$$J_{sc} \propto I^{\alpha}$$

where α depends on recombination loss mechanisms. The photocurrent of an OPV system limited only by geminate recombination would scale linearly with light intensity, giving α=1. The deviation of α from unity to lower values indicates the existence of non-geminate recombination losses. In figure 2(a), the log-log plot of J_{sc} *vs* incident light intensity is shown. The α values as a function of thermal annealing temperatures are respectively, 0.977±0.011 (RT), 0.971±0.009 (70 °C), 0.961±0.008 (100 °C), 0.962±0.013 (120 °C) and 0.951±0.016 (150 °C). This shows that bimolecular recombination is weak and changes little with thermal annealing temperature. [31, 32]

To identify the contribution of different non-geminate recombination losses that prevails in blend films, the dependence of open circuit voltage V_{oc} incident light intensity I was measured and compared to the relation:

$$V_{oc} = \frac{nk_BT}{q} \ln I$$

where n is the recombination *ideality factor* and $\frac{k_BT}{q}$ the thermal voltage. When the slope of V_{oc} *vs* the logarithm of light intensity I is $\frac{k_BT}{q}$, (corresponding to $n = 1$) it indicates bimolecular recombination whereas a steeper slope ($n > 1$) indicates trap assisted recombination.

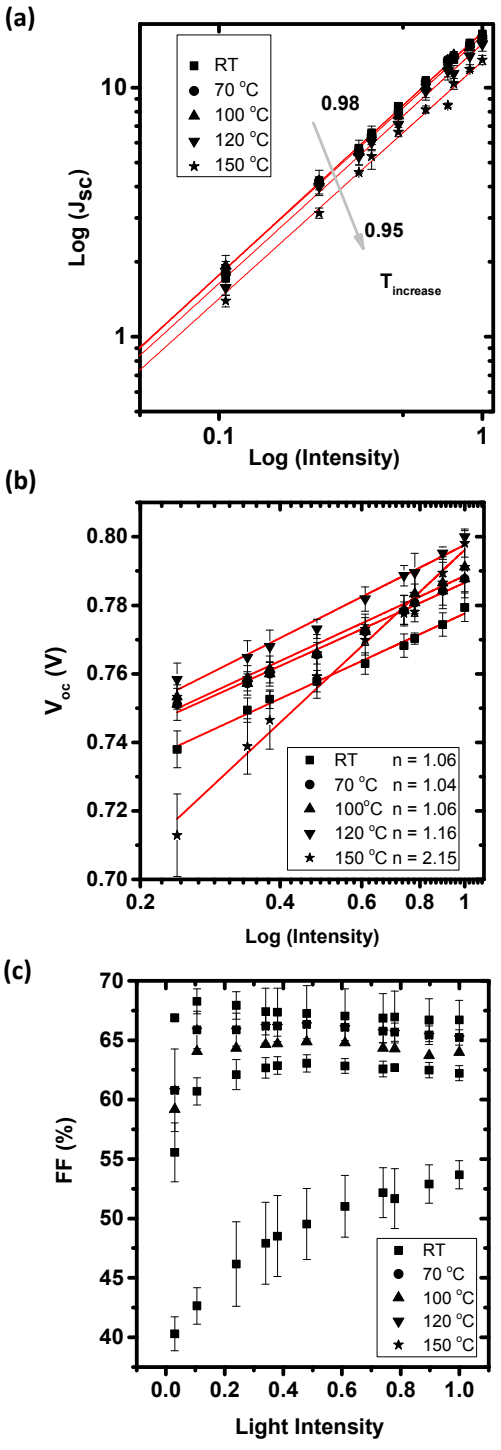

Figure 2. (a) J_{sc} vs Light intensity, fitted to a power law relationship (b) V_{oc} vs Light intensity (c) FF vs Light intensity of the PTB7-Th:$PC_{71}BM$ solar cell devices as a function of thermal annealing.

View Article Online
DOI: 10.1039/C7TA03144K

Figure 2(b) shows V_{oc} variation vs logarithm of light intensity for PTB7-Th:$PC_{71}BM$ blends as a function of thermal annealing. It is interesting to note that up to 100 °C, the $\boldsymbol{n}$ values remain close to unity, then starts to deviate from unity (1.16) for the blend annealed at 120 °C and is highest for 150 °C annealed sample where the slope gives $\boldsymbol{n}$ equal to 2.15. Thus, the main non-geminate recombination loss is bimolecular for the blends annealed up to a temperature of 120 °C and the contribution of trap assisted recombination is dominating for 150 °C annealed blend. Any non-geminate recombination event is effectively eliminating charge carriers that could otherwise contribute to a photocurrent. Hence the drop in J_{sc} with increase in thermal annealing, especially at higher temperatures can be attributed to the loss of photogenerated e-h pairs due to non-geminate recombination.

In Figure 2c, the variation of FF as a function of light intensity is shown. For the blend films annealed up to 120 °C, the FF increases with lowering of light intensity, and for the blends annealed at 150 °C, the FF follows a monotonic decrease with decrease in light intensity. The drop in FF at low light intensities suggests that carrier loss by recombination is significant in PTB7-Th:$PC_{71}BM$ blends annealed at a temperature of 150 °C. The factors that lead to non-geminate recombination are inconsistent pathways of donor/acceptor islands due to phase separation, electron/hole mobility mismatch and increased energetic disorder. Since these factors are correlated to each other, a careful and systematic investigation is carried out to elucidate the contribution of each factor to the observed PCE drop.

Surface morphology of the blends by atomic force microscopy (AFM)

To identify the morphological stability of the PTB7-Th:$PC_{71}BM$ blends to thermal annealing, morphological features were characterised as a function of different annealing temperatures using atomic force microscopy. Time resolved photoluminescence quenching was used as a complementary probe for estimating the domain size[33, 34] and is described at the end of the next section. The morphology of the donor/acceptor network is crucial in maximising efficiency as the carrier lifetime is largely controlled by nanoscale phase morphology between the donor and acceptor materials. Figure S1 and Figure 3(a)-(d) show the AFM height and phase images of PTB7-Th:$PC_{71}BM$ films annealed at different temperatures respectively. The RMS surface roughness [Figure 3e], estimated from statistical distribution of surface height from an area of 10 x 10 μm^2, shows an overall increasing trend. At room temperature, the OPV blend has a surface roughness of ~ 1.8 nm, which increases to ~ 3.2 nm for 150 °C thermally annealed blend. During the intermediate temperature range of 75 °C to 120 °C, the surface roughness remains more or less the same. This could be related to the phase separation of the donor/acceptor blend as the annealing temperature is raised from room temperature to 150 °C, increasing the molecular mobility.

As shown in the AFM phase images (Figure 3), the contrast as well as the size of the bright spots (which correspond to PCBM aggregates due to its high elastic modulus) is increased with thermal annealing temperature indicating that there is an enhancement of PCBM aggregation/phase separation length scale. The phase images of the blends annealed at 75 and 120 °C shows high-contrast interpenetrating channels , while that of 100 and 150 °C show a more gradual and random structure with interspersed

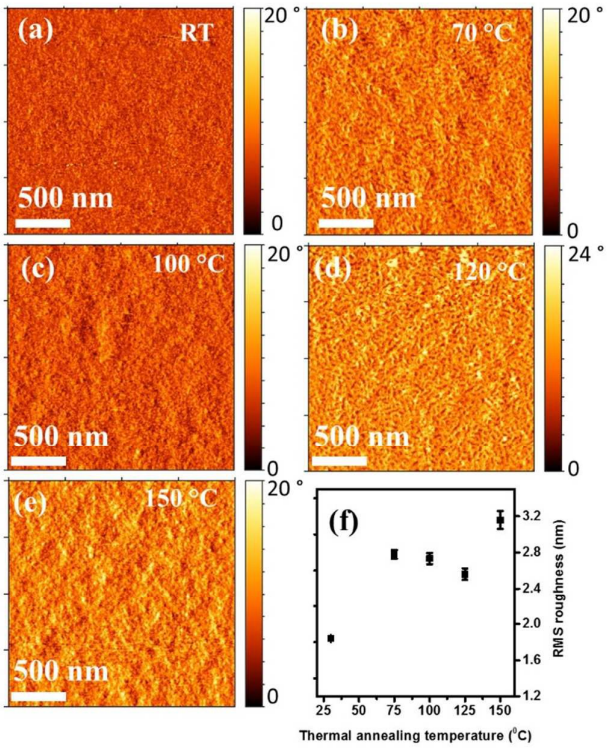

Figure 3. (a)-(e): Atomic force microscopy phase images of the PTB7-Th:$PC_{71}BM$ blends as a function of thermal annealing (f) RMS surface roughness as a function of thermal annealing temperatures.

bright spots. The non-monotonic nature of these patterns makes it difficult to draw detailed, quantitative conclusions regarding the domain size distribution. At room temperature, very low contrast is observed, indicating a fine mixing of the donor acceptor blend, whereas for the blend films annealed at 150 °C, a coarse morphology with large scale phase separation is observed. The distribution of the domain size estimated from AFM height images of the RT and 150 °C processed PTB7-Th:$PC_{71}BM$ blend films are shown in Figure S2. As seen, the average domain size increases from 16 to 20 nm and the FWHM of normal distribution increases from 8 to 10.4 nm as the annealing temperature is increased to 150 °C. The slight increase in FWHM indicates the existence of domains with a varied range of sizes due to thermal annealing at high temperatures. This clearly demonstrates that, donor and/or acceptor molecular motion happens with thermal annealing and corresponding morphological changes are occurring.

Large-scale, unfavorable phase separation in BHJ blends would reduce the probability of photo-generated excitons to arrive at a donor-acceptor interface for their dissociation prior to recombining compared to the system in which donor and acceptor phases are homogeneously distributed. This would reduce the photo-generated current (and hence the J_{sc}). Moreover when free photo-generated electrons and holes transport through the isolated domains of donor and/or acceptor, the probability of recombination with trapped carriers within the hopping/tunneling distance also increases. Thus the reduced J_{sc} and FF of the OPV

View Article Online
DOI: 10.1039/C7TA03144K

blends with increase in thermal annealing temperature can be attributed to the reduced exciton dissociation and increased recombination losses due to inconsistent and unfavorable phase separation. To validate this inference drawn from morphological measurements, detailed photo-physical characterisations of the blend films were performed as described below.

Photophysics of the PTB7-Th:$PC_{71}BM$ blend as a function of thermal annealing

In order to get insight on how the thermal annealing influences the optical properties and exciton/charge dynamics of the PTB7-Th:$PC_{71}BM$ blend, various spectroscopic techniques such as UV-Vis absorption, steady state and time resolved PL spectroscopy are applied. The UV-Vis absorption spectrum shown in Figure 4(a) reveals that due to thermal annealing, PTB7-Th:$PC_{71}BM$ blend does not exhibit any strong blue shift or redshift of the absorption maxima. This observation clearly reveals that the photocurrent drop as a function of thermal annealing is not due to a change in absorption properties of the blend films. To investigate the photo-induced charge transfer between the donor and acceptor molecules, static and dynamic PL spectra of pristine and blend films are recorded. The steady state photoluminescence from pristine PTB7-Th, $PC_{71}BM$ and their blends as a function of thermal annealing are shown in Figure 4(b). The PL emission from PTB7-Th is mainly peaked at 760 nm and from $PC_{71}BM$ at 720 nm, matching well with the previous reports on PL emission[35, 36] for these materials. The PL spectrum of the blend is constituted by combination from both $PC_{71}BM$ and PTB7-Th and no additional peak due to a CT state is observed in the long wavelength region for the analyzed spectral range. This is in contrast to PCDTBT:$PC_{71}BM$ blend where a CT state emission peak is clearly observed. The absence of CT state emission indicates that the CT intermediate state density is too low or that the energy is too close to the PL peak.

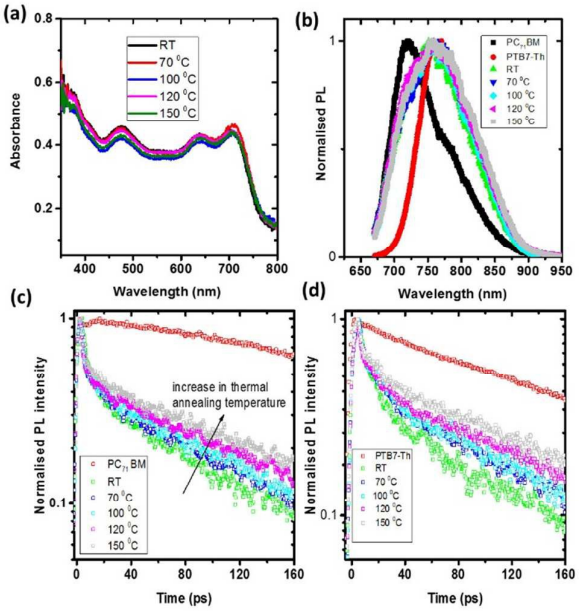

Figure 4. (a) UV-Vis absorption spectra and (b) normalised PL spectra of PTB7-Th:$PC_{71}BM$ blend films as a function of thermal annealing; (c) time resolved PL of the blend detected between 670 nm and 720 nm, which is dominated by emission from fullerene; and (d) time resolved PL of the blend detected between 815 nm and 900 nm, which is dominated by emission from the polymer.

PL quenching provides direct evidence for exciton dissociation, and the degree of PL quenching reflects the efficiency of the exciton charge separation which in turn influences the J_{sc} value of the organic solar cells.[37] A comparison of the PL intensity of the PTB7-Th:$PC_{71}BM$ blend prepared at room temperature and 150 °C is given in Figure S3(a). A reduced exciton quenching efficiency for the blend films annealed at 150 °C is observed in comparison to the room temperature processed blend films. To further confirm this, time resolved PL measurements of the neat and blend films were performed. The PL decay dynamics for the neat PTB7-Th and neat $PC_{71}BM$ are shown in Figure S3 (b). For the case of neat $PC_{71}BM$, the PL decay is mono-exponential with lifetime of ~ 640 ps (corresponding fit to PL decay is given in Figure S3 (b)), whereas the PL decay of pristine PTB7-Th is bi-exponential with a 1/e lifetime of ~ 280 ps. As shown in Figure 4 (b), both PTB7-Th and $PC_{71}BM$ contributed to PL of blend in contrast to previous studies of PTB7 and $PC_{71}BM$ blends where only emission from $PC_{71}BM$ was observed[33]. In order to separate the PTB7-Th and $PC_{71}BM$ emissions, we measured the PL excitation spectra of PTB7-Th:$PC_{71}BM$ blend film at different emission wavelengths (see Figure S4) and observed the contributions from both donor and acceptor molecules. We found that for λ_{em} > 815 nm, emission was mainly from PTB7-Th and for λ_{em} < 720 nm, only $PC_{71}BM$ was emitting. In between these wavelengths, both materials emit. Therefore for our analysis we selected PL decays between 670 and 720 nm for the $PC_{71}BM$ and between 820 and 900 nm for PTB7-Th.

The corresponding PL decays as a function of thermal annealing for the case of $PC_{71}BM$ and PTB7-Th are shown in Figure 4c and 4d respectively. The PL decays of blend films in both cases are faster compared to decays of their corresponding neat films and this is likely due to charge transfer or resonant energy transfer between the well intermixed donor and acceptor molecules in the blend. We extracted quenching efficiency using the previously reported fitting approach[33, 38]

$$\phi_q = 1 - \frac{\int I_{blend}\, dt}{\int I_{neat}\, dt}$$

where I_{blend} and I_{neat} are PL intensity decays of blend and neat films respectively. The obtained values are given in Table S1. The reduced exciton quenching (both in steady state and time resolved PL) of the blend films annealed at 150 °C is accompanied by a reduction in J_{sc} from the thermally annealed blends. The reduced exciton quenching can be due to the increase in length scale of phase separation of the donor-acceptor in the blend. This observation is in agreement with the findings from AFM phase and height images shown in Figure 3 and Figure S1.

Since all blend films have bi-exponential decays (very fast decay at an early time and slower decay at a later time), the lifetimes were estimated from PL decay when they fall to 1/e of their initial value and are given as a function of thermal annealing in Table S2. The corresponding fitted PL decay curves are given in Figure S5 (a) and (b). The 1/e lifetime in both cases increased systematically with increase in thermal annealing and indicates decreasing exciton dissociation efficiency at the polymer: fullerene interfaces after the photoexcitation. This is likely due to an increased domain size resulting in fewer singlet excitons reaching a hetero-interface during their migration. This interpretation is supported by the

View Article Online
DOI: 10.1039/C7TA03144K

increase in feature sizes and surface roughness in AFM seen in Figures 3 and S1. [33, 35]

In order to get quantitative information about the size of $PC_{71}BM$ domains, we used a similar approach to Hedley et al[33] and used the relation,

$$PL_{ratio} = 0.61 \times \sum_{m=1}^{\infty} \exp\left(\frac{-D\pi^2 m^2 t}{r^2}\right)$$

Where D is the diffusion coefficient, PL_{ratio} is the ratio of the PL of the blend (detected between 670 nm and 720 nm) and the PL of the neat $PC_{71}BM$ film, r is radius of the PCBM domain, and t is time. For our analysis we used the previously reported value of $D = 1.6 \times 10^{-4} cm^2/s$ for $PC_{71}BM$.[33] At the earliest times, fast decay is due to direct energy transfer. Therefore we fitted the ratio of PL decays of blend and pristine film in the region > 8 ps (where PL decay is mainly due to exciton diffusion) and found that the size of pure domains of $PC_{71}BM$ increased with annealing temperature (Table S2 and Figure S6). Compared to the domain size estimated from the AFM height images (Figure S2), the domain size estimated from the PL decay studies is smaller and this difference in size estimation could be due to the difference in the assumptions and resolutions achievable with the two different methods.

Thus both steady state and time resolved PL spectroscopic measurements imply a reduced exciton dissociation efficiency due to increased domain size in the blend films with increase in thermal annealing temperature. This can be due to the coarse phase-separation of the donor-acceptor blend films with increase in thermal annealing temperature, reducing the interfacial area between the donor PTB7-Th and acceptor $PC_{71}BM$ leading to a suppression of density of initially photo-generated charge carriers. Thus the decrease in short circuit density of the PTB7-Th:$PC_{71}BM$ solar cells with increase in thermal annealing temperatures can be due to the increased domain size of the components in the blend films. Previously Guo et al[39] have reported similar observation of reduced interfacial boundaries in thermally annealed PTB1:PCBM films thereby dropping the solar cell PCE by ~ 60%. The main factor that contributed to the drop in PCE was the lowered Jsc because of the reduced exciton splitting in annealed blend films due to the larger PCBM domains.

So far the thermal annealing induced morphological and photophysical properties of PTB7-Th:$PC_{71}BM$ blend films and their correlation to the observed photovoltaic performance, with a focus on short circuit current density, were discussed. In the following section, the molecular packing and the crystallinity of the blend films due to thermal annealing and its correspondence to other photovoltaic properties of Voc and FF are discussed.

Structural properties by GIWAXS data analysis

To identify how the thermal annealing changes the molecular packing of both the donor and the acceptor, GIWAXS studies were performed on thermally annealed blend films. Figure 5 shows the GIWAXS 2D patterns of the PTB7-Th:$PC_{71}BM$ blend as a function of thermal annealing. After applying necessary geometry corrections, we can identify three peaks typical of $PC_{71}BM$ (at Q=0.7, 1.36, and 1.96 $Å^{-1}$) and peaks associated with the polymer alkyl stacking peak (Q=0.32 $Å^{-1}$) [corresponding to (100) Bragg reflection] and the polymer π-stacking peak (Q=1.6 $Å^{-1}$)[30, 40] [corresponding to (001) Bragg reflection]. The alkyl stacking peak is more intense in the in-plane direction, and the π-stacking peak is prominent in the out-of-plane direction, showing a preferential face-on orientation. With increase in thermal annealing, the alkyl peak becomes more intense relative to the PCBM diffraction, suggesting a slight increase in ordering of PTB7-Th donors. No orientation change of the donor molecules with increase in thermal annealing is observed. A previous study on X-ray scattering of P3HT:PCBM blend and photocurrent has revealed that J_{sc} depends more on the local ordering of the PCBM than on the π-stacking of the donor molecule[41]. Even though the degree of crystallinity of the PTB7-Th donors increases with thermal annealing, in contrast to P3HT which shows greatly improved ordering on annealing, the J_{sc} of the devices drops systematically with increase in annealing temperature.[42] The $PC_{71}BM$ scattering is observed as broad diffusive rings (at 0.6 and 1.4 $A^{\circ -1}$), indicating a disordered amorphous or nanocrystalline state. The PCBM ring intensity increases with temperature indicating increase in aggregation of PCBM. This observation is in agreement with AFM height and phase imaging in Figure 3 and Figure S1, and photophysical analysis shown in Figure 4, where the increase in phase purity and domain size with increase in thermal annealing temperature is clearly visible. Normalising the GIWAXS data by the second PCBM scattering peak reveals that the polymer alkyl diffraction grows faster than the PCBM aggregates [Figure S7]. This could be due to PCBM diffusion out of mixed regions, forming weak PCBM aggregates and allowing the polymer to crystallize strongly. The improved photovoltage observed for the thermally annealed PTB7-Th:$PC_{71}BM$ blend can be related to the improved crystallinity of the PTB7-Th donor molecule which would reduce the energetic disorder/defect states, resulting in downshifting of the hole fermi level[43]. Recently, Gonzalez et al[44] have reported direct evidence for how the increased crystallinity of the donor polymer (P3HT) in the active layer can contribute to enhanced photovoltage in a BHJ OPV by using an *in-operando* combination of GIWAXS and I–V tracking.

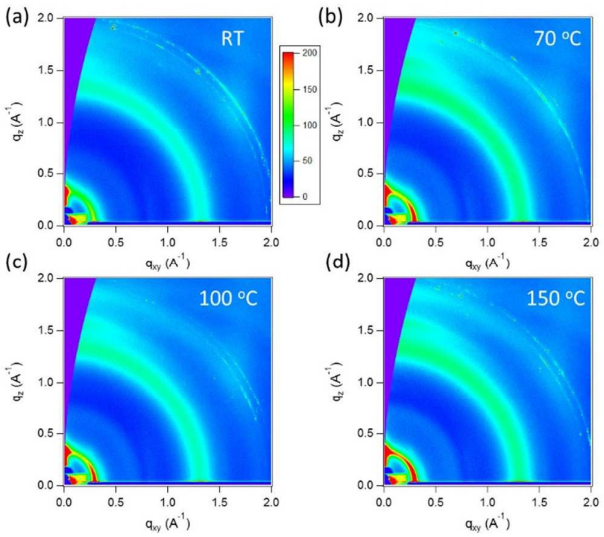

Figure 5. (a)-(d): GIWAX 2D patterns of the PTB7-Th:$PC_{71}BM$ blend films as a function of thermal annealing.

Space charge limited current (SCLC) mobility measurements

The photovoltaic properties of the polymer blend films are highly correlated to the charge transport properties. In order to

View Article Online
DOI: 10.1039/C7TA03144K

obtain high fill factor for OPVs, balanced and high charge carrier mobilities are required for holes and electrons. To study how the thermal annealing is affecting the charge transporting properties of the PTB7-Th:$PC_{71}BM$ blend, the hole and electron mobility in the blend films are estimated using the space charge limited current (SCLC) method. The structure of hole only devices are ITO/PEDOT:PSS/PTB7-Th:$PC_{71}BM$/MoO_3/Ag and Al/PTB7-Th:$PC_{71}BM$/LiF/Al respectively (Figure S8). The J-V curves of the devices made with blend films annealed at different temperatures are shown in Figure 6. The mobility of holes and electrons are estimated using the Mott-Murgatroyd relation[45]:

$$J_{sclc} = \frac{9}{8}\varepsilon\frac{(V-V_b)^2}{d^3}\mu_0 \exp\left(0.89\gamma\sqrt{\frac{(V-V_b)}{d}}\right)$$

where J_{sclc} is the steady state current density function of applied voltage V; d is the film thickness, ε is the dielectric constant of the organic semiconductors (set as 3.5), and μ_0 represents the mobility in the limit of zero electric field, V_b the built in voltage and γ the electric field dependent factor**.** As given in Table 2, with increase in thermal annealing there is no considerable variation in hole/electron mobility. However, for the blend films annealed at 150 °C, the charge mobility imbalance is highest. This charge mobility imbalance can cause space charge effects in the active layer blend impeding the charge extraction processes and promoting the trap- assisted recombination losses.[46] This is in accordance with the inference drawn from the recombination losses studies shown in Figure 2b, where the 150 °C annealed blend films showed the highest recombination losses. Thus the drop in Jsc and FF observed for the PTB7-Th:$PC_{71}BM$ blends with increase in thermal annealing temperatures can be summarized as due to reduced exciton dissociation due to large length scale phase separation and increased recombination losses.

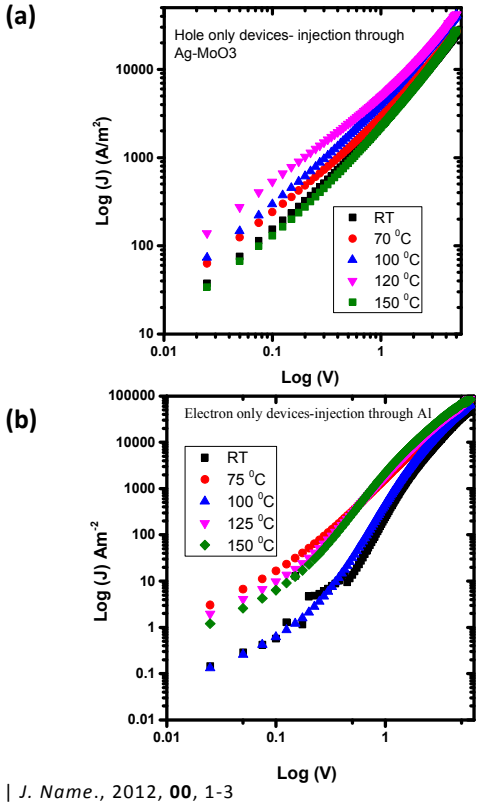

Figure 6. (J-V) characteristics of the hole only (a) and electron only devices (b) of the PTB7-Th:$PC_{71}BM$ blend films annealed at various temperatures.

Table 2: Electron and hole mobility of the PTB7-Th:$PC_{71}BM$ blend system as a function of thermal annealing.

Annealing temperature (°C)	Hole mobility ($cm^2V^{-1}s^{-1}$)	Electron mobility ($cm^2V^{-1}s^{-1}$)	$\frac{\mu_e}{\mu_h}$
RT	$8.6\pm1.7 \times 10^{-4}$	$2.14\pm0.32 \times 10^{-3}$	2.5±0.62
75	$9.0\pm0.4 \times 10^{-4}$	$2.26\pm0.59 \times 10^{-3}$	2.51±0.66
100	$10.1\pm1.6 \times 10^{-4}$	$2.38\pm0.40 \times 10^{-3}$	2.35±0.55
125	$10.6\pm2.1 \times 10^{-4}$	$2.45\pm0.55 \times 10^{-3}$	2.31±0.68
150	$8.5 \pm2.1 \times 10^{-4}$	$3.10 \pm0.15 \times 10^{-3}$	3.64±0.74

Based on the above described morphological and optoelectronic characterization, the critical factor that leads to the photovoltaic performance degradation of thermally annealed PTB7-Th: $PC_{71}BM$ blend films is increased domain size of the donor : acceptor components. Figure 7 shows a schematic of what happens to the PTB7-Th:$PC_{71}BM$ BHJ blends on thermally annealing at 150 °C. The correlation of morphological degradation on a nanometre scale and the photovoltaic performance for P3HT:PCBM and PCDTBT:$PC_{71}BM$ solar cells under continuous illumination of ~18 h and *in-operando* condition has been previously reported by Schaffer et al,[24, 25] where the authors employed GISAXS to probe the microstructural evolution of the BHJ active layer. Though solar cell performance loss is attributed to morphological instability, depending on the active layer blend, different responses in photovoltaic performance parameters and microstructure evolution with time were observed. In the case of P3HT : PCBM solar cells, growth of the domain size of the active layer components was observed whilst in PCDTBT:$PC_{71}BM$ solar cells, domain size shrank. Hence, for P3HT:PCBM solar cells, the highest drop was observed in Jsc, (due to reduced exciton splitting) with smaller changes in Voc and FF. In contrast, for PCDTBT : $PC_{71}BM$, the shrinking leads to a loss of connectivity in the interpenetrating network and hence a drop in FF played the largest role in solar cell performance degradation. In the present case of thermally annealed PTB7-Th: $PC_{71}BM$ blend based solar cells, the increased domain size caused a reduction in exciton splitting as discussed in the photophysics section, and hence a higher drop is observed in Jsc (16 %) than in FF (11 %). The increased crystallinity of the PTB7-Th and small effects of thermal annealing on electron/hole mobility are possible reasons for the relatively low drop in FF. Thus, while discussing the performance degradation of OPVs due to morphology instability, these two different morphological aspects should be taken into consideration and based on the response of the PV performance parameters, structural changes can be inferred.

View Article Online
DOI: 10.1039/C7TA03144K

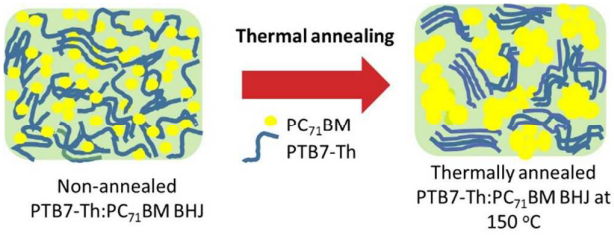

Figure 7: Schematic illustration of morphological changes happening to PTB7-Th:$PC_{71}BM$ blend films on thermal annealing.

Thermally annealed blends using non-fullerene acceptors

Since, morphological instability was the main reason for the adverse photovoltaic properties of the PTB7-Th:$PC_{71}BM$ blends annealed at higher temperatures, we were motivated to test the photovoltaic properties of a non-fullerene acceptor based blend system at similar conditions. The recently reported non-fullerene small molecule acceptor ITIC was selected to investigate the thermal stability of the blend[47, 48]. ITIC is based on a bulky seven-ring fused core (indacenodithieno[3,2-b]thiophene, IT), with 2-(3-oxo-2,3-dihydroinden-1-ylidene)malononitrile (INCN) groups end-capped to the ring, and with four 4-hexylphenyl groups substituted on it [Figure 8a]. These four rigid 4-hexylphenyl substituents are reported to restrict molecular planarity, aggregation, and large phase separation in non-fullerene BHJ blend films[47]. The OPV device performance as a function of thermal annealing is given in Table 3 and Figure 8. It should be noted that the PCE of this blend system is not as high as the $PC_{71}BM$-based system and more optimisation process are underway. The PCE only drops by 9% of its as-spun value for an increase in thermal annealing from room temperature to 150 °C, while the $PC_{71}BM$ based fullerene acceptor blend showed a PCE drop of 30 %. Similarly to PCBM based systems, the EQE spectra (Figure 8(c)) of the PTB7-Th: ITIC OPVs do not show considerable difference as a function of thermal annealing.

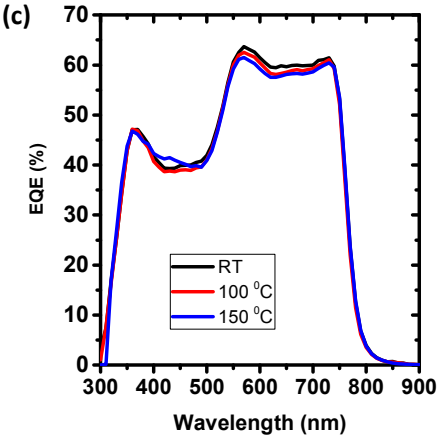

Table 3: Photovoltaic performance of PTB7-Th:ITIC blend films as a function of thermal annealing. For each annealing temperature, the first row shows average photovoltaic parameters of 7 devices (and the standard deviation) and second row shows the best device.

Annealing Temp. (°C)	J_{sc} (mA/cm²)	V_{oc} (V)	FF (%)	PCE avg. (%)	PCE best (%)
RT	15.2(0.3)	0.78(0.01)	49.0(1.7)	5.8(0.3)	
	15.7	0.78	51.7		6.3
100	15.0(0.2)	0.77(0.01)	46.7(0.7)	5.4(0.1)	
	15.3	0.77	48.2		5.70
150	14.8(0.5)	0.77(0.01)	45.5(0.3)	5.2(0.2)	
	15.2	0.78	45.8		5.45

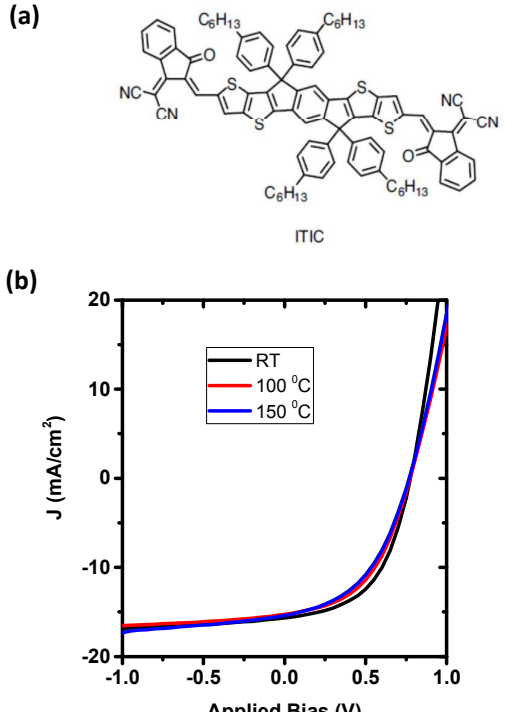

Figure 8. (a) Molecular structure of the non-fullerene acceptor ITIC (b) J-V characteristics (c) EQE spectra of the PTB7-Th:ITIC blend as a function of thermal annealing temperature.

To compare how the thermal annealing affects the morphology of the PTB7-Th: ITIC blend, atomic force microscopy images of the blend films at RT and annealed at 150 °C were measured and are shown in Figure 9. The AFM height images are shown in Figure 9(a) and (b), whereas the corresponding phase images are shown in Figure 9(c) and 9(d). Homogeneous mixing of the donor and acceptor molecules are evident from these images. No considerable difference in domain size or length scale of phase separation is observed either from the AFM height or phase images due to thermal annealing at 150 °C. This is in accordance with the observed RMS roughness values for the RT and thermally annealed blends, which are respectively 2.6 nm and 2.5 nm. This is in contrary to PTB7-Th:$PC_{71}BM$ blend where thermally annealing process increases the RMS roughness [Figure 3(e)]. The retention of the photovoltaic properties of the PTB7-Th: ITIC blend films even after annealing at 150 °C can be attributed to its morphological stability.

View Article Online
DOI: 10.1039/C7TA03144K

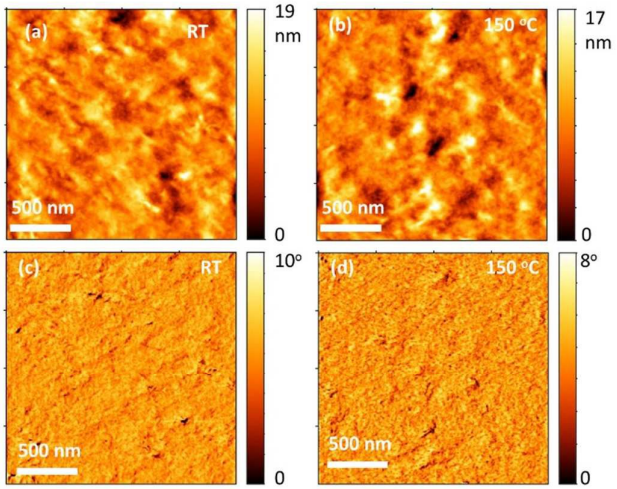

Figure 9. Atomic force microscopy height images of PTB7-Th:ITIC films at (a) RT and (b) thermally annealed at 150 °C. The corresponding AFM phase images are shown in (c) and (d).

Conclusion

The effect of thermal annealing on the photovoltaic properties of a highly efficient BHJ system comprised of PTB7-Th:$PC_{71}BM$ is investigated. The decrease in power conversion efficiency, reflected mainly through a drop in Jsc and FF, is identified as due to the suppression of exciton dissociation and increased recombination losses induced by morphological instability with increase in thermal annealing temperature. However, the improved ordering of the PTB7-Th donor molecule with thermal annealing resulted in an enhanced open circuit voltage. By replacing the fullerene $PC_{71}BM$ acceptor by non-fullerene acceptor molecule of ITIC, improved morphological stability is observed and hence better retention of the photovoltaic performance as a function of thermal annealing is obtained. This result strengthens the need to develop BHJ systems with morphological stability and stable acceptor molecules along with the development of highly efficient, narrow band gap donor molecules.

Acknowledgements:

We acknowledge support from EPSRC (grant number EP/L012294/1) and the European Research Council (grant number 321305). I.D.W.S. also acknowledges a Royal Society Wolfson Research Merit Award. VS acknowledges support from the Office of Naval Research NDSEG fellowship. Use of the Stanford Synchrotron Radiation Lightsource, SLAC National Accelerator Laboratory, is supported by the U.S. Department of Energy, Office of Science, Office of Basic Energy Sciences under Contract No. DE-AC02-76SF00515. We thank Stefan Oosterhout for valuable discussions.

Data

Research data supporting this paper is available at doi http://dx.doi.org/10.17630/eadf56f3-8c70-47da-ac6d-67f2d78b3f74

References

1. Lu, L. Y.; Zheng, T. Y.; Wu, Q. H.; Schneider, A. M.; Zhao, D. L.; Yu, L. P. *Chemical Reviews* **2015,** 115, (23), 12666-12731.
2. Abdulrazzaq, O. A.; Saini, V.; Bourdo, S.; Dervishi, E.; Biris, A. S. *Particulate Science and Technology* **2013,** 31, (5), 427-442.
3. Khalil, A.; Ahmed, Z.; Touati, F.; Masmoudi, M. In *Review on organic solar cells*, 2016 13th International Multi-Conference on Systems, Signals & Devices (SSD), 21-24 March 2016, 2016; pp 342-353.
4. Dou, L. T.; You, J. B.; Hong, Z. R.; Xu, Z.; Li, G.; Street, R. A.; Yang, Y. *Advanced Materials* **2013,** 25, (46), 6642-6671.
5. Chen, J. D.; Cui, C. H.; Li, Y. Q.; Zhou, L.; Ou, Q. D.; Li, C.; Li, Y. F.; Tang, J. X. *Advanced Materials* **2015,** 27, (6), 1035-1041.
6. Liu, C.; Yi, C.; Wang, K.; Yang, Y.; Bhatta, R. S.; Tsige, M.; Xiao, S.; Gong, X. *ACS Applied Materials & Interfaces* **2015,** 7, (8), 4928-4935.
7. He, Z.; Xiao, B.; Liu, F.; Wu, H.; Yang, Y.; Xiao, S.; Wang, C.; Russell, T. P.; Cao, Y. *Nat Photon* **2015,** 9, (3), 174-179.
8. Jagadamma, L. K.; Al-Senani, M.; El-Labban, A.; Gereige, I.; Ndjawa, G. O. N.; Faria, J. C. D.; Kim, T.; Zhao, K.; Cruciani, F.; Anjum, D. H.; McLachlan, M. A.; Beaujuge, P. M.; Amassian, A. *Adv. Energy Mater.* **2015,** 5, (12), 12.
9. Liu, J.; Durstock, M.; Dai, L. *Energy & Environmental Science* **2014,** 7, (4), 1297-1306.
10. Zhao, J.; Li, Y.; Yang, G.; Jiang, K.; Lin, H.; Ade, H.; Ma, W.; Yan, H. *Nature Energy* **2016,** 1, 15027.
11. Liao, S.-H.; Jhuo, H.-J.; Yeh, P.-N.; Cheng, Y.-S.; Li, Y.-L.; Lee, Y.-H.; Sharma, S.; Chen, S.-A. *Scientific Reports* **2014,** 4, 6813.
12. Zhao, W. C.; Qian, D. P.; Zhang, S. Q.; Li, S. S.; Inganas, O.; Gao, F.; Hou, J. H. *Advanced Materials* **2016,** 28, (23), 4734-4739.
13. Nam, S.; Seo, J.; Woo, S.; Kim, W. H.; Kim, H.; Bradley, D. D. C.; Kim, Y. *Nat Commun* **2015,** 6.
14. Jorgensen, M.; Norrman, K.; Krebs, F. C. *Solar Energy Materials and Solar Cells* **2008,** 92, (7), 686-714.
15. Tada, K. *Solar Energy Materials and Solar Cells* **2015,** 132, 15-20.
16. Balcaen, V.; Rolston, N.; Dupont, S. R.; Voroshazi, E.; Dauskardt, R. H. *Solar Energy Materials and Solar Cells* **2015,** 143, 418-423.
17. Pearson, A. J.; Hopkinson, P. E.; Couderc, E.; Domanski, K.; Abdi-Jalebi, M.; Greenham, N. C. *Organic Electronics* **2016,** 30, 225-236.
18. Owens, C.; Ferguson, G.; Hermenau, M.; Voroshazi, E.; Galagan, Y.; Zimmermann, B.; Rösch, R.; Angmo, D.; Teran-Escobar, G.; Uhrich, C.; Andriessen, R.; Hoppe, H.; Würfel, U.; Lira-Cantu, M.; Krebs, F.; Tanenbaum, D. *Polymers* **2016,** 8, (1), 1.
19. Roesch, R.; Faber, T.; von Hauff, E.; Brown, T. M.; Lira-Cantu, M.; Hoppe, H. *Advanced Energy Materials* **2015,** 5, (20), 1501407-n/a.
20. Jagadamma, L. K.; Al-Senani, M.; El-Labban, A.; Gereige, I.; Ndjawa, G. O. N.; Faria, J. C. D.; Kim, T.; Zhao, K.; Cruciani, F.; Anjum, D. H.; McLachlan, M. A.; Beaujuge, P. M.; Amassian, A. *Advanced Energy Materials* **2015,** 5, (12).
21. Norrman, K.; Madsen, M. V.; Gevorgyan, S. A.; Krebs, F. C. *Journal of the American Chemical Society* **2010,** 132, (47), 16883-16892.
22. Wang, X. Z.; Zhao, C. X.; Xu, G.; Chen, Z. K.; Zhu, F. R. *Solar Energy Materials and Solar Cells* **2012,** 104, 1-6.
23. Tremolet de Villers, B. J.; O'Hara, K. A.; Ostrowski, D. P.; Biddle, P. H.; Shaheen, S. E.; Chabinyc, M. L.; Olson, D. C.; Kopidakis, N. *Chemistry of Materials* **2016,** 28, (3), 876-884.

View Article Online
DOI: 10.1039/C7TA03144K

24. Schaffer, C. J.; Palumbiny, C. M.; Niedermeier, M. A.; Burger, C.; Santoro, G.; Roth, S. V.; Müller-Buschbaum, P. *Advanced Energy Materials* **2016,** 6, (19), 1600712-n/a.
25. Schaffer, C. J.; Palumbiny, C. M.; Niedermeier, M. A.; Jendrzejewski, C.; Santoro, G.; Roth, S. V.; Müller-Buschbaum, P. *Advanced Materials* **2013,** 25, (46), 6760-6764.
26. Li, G.; Shrotriya, V.; Huang, J.; Yao, Y.; Moriarty, T.; Emery, K.; Yang, Y. *Nat Mater* **2005,** 4, (11), 864-868.
27. Mihailetchi, V. D.; Xie, H. X.; de Boer, B.; Koster, L. J. A.; Blom, P. W. M. *Advanced Functional Materials* **2006,** 16, (5), 699-708.
28. Jagadamma, L. K.; Abdelsamie, M.; El Labban, A.; Aresu, E.; Ngongang Ndjawa, G. O.; Anjum, D. H.; Cha, D.; Beaujuge, P. M.; Amassian, A. *Journal of Materials Chemistry A* **2014,** 2, (33), 13321-13331.
29. Synooka, O.; Eberhardt, K.-R.; Singh, C. R.; Hermann, F.; Ecke, G.; Ecker, B.; von Hauff, E.; Gobsch, G.; Hoppe, H. *Advanced Energy Materials* **2014,** 4, (5), n/a-n/a.
30. Bartelt, J. A.; Beiley, Z. M.; Hoke, E. T.; Mateker, W. R.; Douglas, J. D.; Collins, B. A.; Tumbleston, J. R.; Graham, K. R.; Amassian, A.; Ade, H.; Frechet, J. M. J.; Toney, M. F.; McGehee, M. D. *Advanced Energy Materials* **2013,** 3, (3), 364-374.
31. Lakhwani, G.; Rao, A.; Friend, R. H., Bimolecular Recombination in Organic Photovoltaics. In *Annual Review of Physical Chemistry, Vol 65*, Johnson, M. A.; Martinez, T. J., Eds. 2014; Vol. 65, pp 557-581.
32. Liu, Y.; Lai, J. Y. L.; Chen, S.; Li, Y.; Jiang, K.; Zhao, J.; Li, Z.; Hu, H.; Ma, T.; Lin, H.; Liu, J.; Zhang, J.; Huang, F.; Yu, D.; Yan, H. *Journal of Materials Chemistry A* **2015,** 3, (26), 13632-13636.
33. Hedley, G. J.; Ward, A. J.; Alekseev, A.; Howells, C. T.; Martins, E. R.; Serrano, L. A.; Cooke, G.; Ruseckas, A.; Samuel, I. D. W. *Nature Communications* **2013,** 4, 2867.
34. Ruseckas, A.; Shaw, P. E.; Samuel, I. D. W. *Dalton Transactions* **2009**, (45), 10040-10043.
35. Zusan, A.; Gieseking, B.; Zerson, M.; Dyakonov, V.; Magerle, R.; Deibel, C. *Scientific Reports* **2015,** 5.
36. Alsulami, Q. A.; Murali, B.; Alsinan, Y.; Parida, M. R.; Aly, S. M.; Mohammed, O. F. *Advanced Energy Materials* **2016,** 6, (11), 7.
37. Hedley, G. J.; Ruseckas, A.; Samuel, I. D. W. *Chemical Reviews* **2017,** 117, (2), 796-837.
38. Aldakov, D.; Sajjad, M. T.; Ivanova, V.; Bansal, A. K.; Park, J.; Reiss, P.; Samuel, I. D. W. *Journal of Materials Chemistry A* **2015,** 3, (37), 19050-19060.
39. Guo, J.; Liang, Y.; Szarko, J.; Lee, B.; Son, H. J.; Rolczynski, B. S.; Yu, L.; Chen, L. X. *The Journal of Physical Chemistry B* **2010,** 114, (2), 742-748.
40. Cheng, P.; Yan, C.; Wu, Y.; Wang, J.; Qin, M.; An, Q.; Cao, J.; Huo, L.; Zhang, F.; Ding, L.; Sun, Y.; Ma, W.; Zhan, X. *Advanced Materials* **2016**, n/a-n/a.
41. Gomez, E. D.; Barteau, K. P.; Wang, H.; Toney, M. F.; Loo, Y. L. *Chemical Communications* **2011,** 47, (1), 436-438.
42. Verploegen, E.; Mondal, R.; Bettinger, C. J.; Sok, S.; Toney, M. F.; Bao, Z. *Advanced Functional Materials* **2010,** 20, (20), 3519-3529.
43. Ripolles, T. S.; Guerrero, A.; Garcia-Belmonte, G. *Applied Physics Letters* **2013,** 103, (24).
44. Moseguí González, D.; Schaffer, C. J.; Pröller, S.; Schlipf, J.; Song, L.; Bernstorff, S.; Herzig, E. M.; Müller-Buschbaum, P. *ACS Applied Materials & Interfaces* **2017,** 9, (4), 3282-3287.
45. Blakesley, J. C.; Castro, F. A.; Kylberg, W.; Dibb, G. F. A.; Arantes, C.; Valaski, R.; Cremona, M.; Kim, J. S.; Kim, J.-S. *Organic Electronics* **2014,** 15, (6), 1263-1272.
46. Stolterfoht, M.; Armin, A.; Philippa, B.; Neher, D. *Journal of Physical Chemistry Letters* **2016,** 7, (22), 4716-4721.
47. Lin, Y.; Wang, J.; Zhang, Z.-G.; Bai, H.; Li, Y.; Zhu, D.; Zhan, X. *Advanced Materials* **2015,** 27, (7), 1170-1174.
48. Zhao, W.; Qian, D.; Zhang, S.; Li, S.; Inganäs, O.; Gao, F.; Hou, J. *Advanced Materials* **2016,** 28, (23), 4734-4739.

View Article Online
DOI: 10.1039/C7TA03144K

TOC Entry

The effect of thermal annealing on a polymer solar cell is investigated and related to changes in the photophysics and structure.

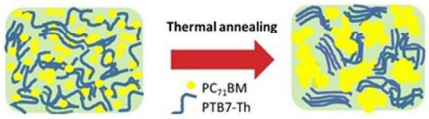

The effect of thermal annealing on a polymer solar cell is investigated and related to changes in the photophysics and structure.

254x190mm (96 x 96 DPI)